Theoretical, Numerical, and Experimental Investigation on Resonant Vibrations of Piezoceramic Annular Disks

Chi-Hung Huang, Chien-Ching Ma, and Yu-Chih Lin

***Abstract*—In this study, vibration characteristics of thin piezoceramic annular disks with stress-free boundary conditions are investigated by theoretical analysis, numerical simulation, and experimental measurement. The nonaxisymmetric, out-of-plane (transverse), and axisymmetric in-plane (tangential and radial extensional) vibration modes are discussed in detail in terms of resonant frequencies, mode shapes, and electrical currents. Two optical techniques, amplitude-fluctuation electronic speckle pattern interferometry (AF-ESPI) and laser Doppler vibrometer (LDV), as well as the electrical impedance measurement are used to validate the analytical results. Both theoretical and experimental results indicate that the transverse and tangential vibration modes cannot be determined by the impedance analysis; hence, only resonant frequencies of extensional vibration modes are presented from the impedance analyzer. The LDV system is used to measure the resonant frequencies of transverse vibrations. However, both the transverse and extensional vibration modes and resonant frequencies of piezoceramic annular disks are obtained by the AF-ESPI method, and the interferometric fringes are produced instantly by a video recording system. Numerical results obtained by finite-element calculations are compared with those from theoretical analysis and experimental measurements. It is shown that the theoretical predictions of resonant frequencies and the corresponding mode shapes agree well with the experimental results. Good agreement between the predicted and measured electrical impedance also is found. The dependence of resonant frequencies and dynamic electromechanical coupling coefficients on the inner-to-outer radius ratio also is analyzed and discussed in this study.**

I. Introduction

MANY modern engineering applications are successfully achieved by using the piezoelectric effect. Piezoelectricity describes the phenomenon in which the material generates electric charge when subjected to stress and, conversely, generates strain when the electric field is applied. Because of their simple configuration and high performance, the piezoelectric materials are widely used in electromechanical sensors, actuators, nondestructive testing devices, and electro-optic modulator. Especially for the piezoelectric ceramics made of lead zirconate titanate (PZT), numerous investigations have been performed on the disk or annulus types in the analysis and applications, e.g., Langevin transducers and ultrasonic motors. The vibration characteristics of piezoelectric materials are determined by the linear piezoelasticity, the Maxwell equation, and piezoelectric constitutive equations [1], [2]. Nevertheless, it is difficult to obtain complete solutions for even a simple geometry. Iula *et al.* [3] proposed a matrix model to study the radial symmetric mode of a thin piezoceramic ring with inner and outer lateral surfaces loaded by the surrounding medium. The resonant frequency spectrum and effective electromechanical coupling coefficient (k_{eff}) were discussed as functions of the inner-to-outer radius ratio. Furthermore, using the previously proposed model, Iula *et al.* [4] defined the material coupling factor (k_{mat}) for the ring geometry to take into account its variation with respect to the inner-to-outer radius ratio. Shuyu [5] found that the thickness-shearing vibration of the tangential polarized piezoceramic ring is related to the shape and dimension of the cross section. From theoretical and experimental investigations, the effect of the cross-sectional shape on the electromechanical coupling coefficient and resonant frequency had been verified. Takano *et al.* [6] used the in-plane nonaxisymmetric vibration modes of a piezoelectric annular plate to investigate the application on an ultrasonic motor. In the analysis of displacement and electromechanical coupling factor, the favorable vibration modes were suggested for different ultrasonic motor configurations. Ha and Kim [7] proposed using the 5×5 impedance and admittance matrices to analyze the vibration characteristics of a symmetric triple-layer piezoelectric annular bimorph (PAB). The resonant frequencies and effective electromechanical coupling factors can be calculated by the five-port impedance matrix that is composed of the mechanical, electrical, and electromechanical coupling impedance matrices. Ha and Kim [8] used the preceding method to carry out the analysis of dynamic behavior for an asymmetric piezoelectric annular bimorph. Because the geometrical configuration of piezoceramic transducers usually is circular, the vibration characteristics of piezoceramic disks are important in transducer design and application. Kunkel *et al.* [9] inves-

Manuscript received March 26, 2004; accepted October 24, 2004. The authors gratefully acknowledge the financial support of this research by the National Science Council (Republic of China) under Grant NSC 91-2212-E-231-002 (C. H. H.) and 90-2212-E-002-163 (C. C. M.).

C. H. Huang is with the Department of Mechanical Engineering, Ching Yun University, Chung-Li, Taiwan 320, Republic of China.

C.-C. Ma is with the Department of Mechanical Engineering, National Taiwan University, Taipei, Taiwan 106, Republic of China (e-mail: ccma@ntu.edu.tw).

Y.-C. Lin is with the Department of Biomedical Engineering, Yuanpei Institute of Science and Technology, Hsinchu, Taiwan 300, Republic of China.

tigated the vibration modes of PZT-5H ceramics disks for the diameter-to-thickness (D/T) ratio ranging from 0.2 to 10. Guo *et al.* [10] presented the results for PZT-5A piezoelectric disks with D/T of 20 and 10. Ivina [11] studied the symmetric modes of vibration for circular piezoelectric plates to determine the resonant and antiresonant frequencies, radial mode configurations, and optimum geometrical dimensions to maximize the dynamic electromechanical coupling coefficient. Most of the works for vibration analysis of piezoelectric plates in the above mentioned literature are analytical and numerical results.

In general, two experimental methods usually are used to study the vibration problem of piezoelectric materials; one is the equivalent circuit measurement (also known as admittance analysis) and the other is the optical interferometric technique. Shaw [12] used an optical interference technique in which a stroboscopically illuminated multiple beam was used to measure the surface motion of thick barium titanate disks. However, only normal modes having symmetry with respect to the axis and to the central plane were observed. Minoni and Docchio [13] proposed an optical self-calibrating technique, which used the signal-processing chain to measure the vibration amplitude of PZT for different operating frequencies. To evaluate the piezoelectric constants, Ohki *et al.* [14] used the fiber-optic technique to measure the vibration amplitude of piezoceramic circular rod and disk. To obtain the vibration-mode shapes simultaneously, the full-field measurement technique should be used. Koyuncu [15] used electron speckle pattern interferometry (ESPI) with reference-beam modulation to measure the vibration amplitudes and vibration modes of PZT-4 transducers in air and water. Oswin *et al.* [16] used ESPI to validate the finite-element model of flextensional transducer with an elliptical shape. Both in-plane and out-of plane vibrations were studied and discussed. Ma and Huang [17] and Huang and Ma [18] used the amplitude-fluctuation (AF)-ESPI method to investigate the three-dimensional vibration of piezoelectric rectangular parallelepipeds and cylinders, and they presented both the resonant frequencies and mode shapes.

For the piezoceramic annular disk polarized in the thickness direction, much research and many applications have been carried out on the extensional (in-plane) vibrations, but only very few results of the transverse (out-of-plane) vibrations are available. There also are very few experimental results for the full-field configuration of mode shapes of vibrating piezoelectric plates available in the literature. If the piezoceramic annular disk is thin, then the out-of-plane (transverse) and two in-plane (tangential and radial extensional) vibrations are decoupled. In this study, the dynamic characteristics for three different types of vibration modes (transverse, tangential, and extensional) for piezoceramic annular disks will be analyzed and discussed. To validate the theoretical results, this study uses two optical techniques: AF-ESPI and laser Doppler vibrometer (LDV), and the electrical impedance measurement to investigate experimentally the vibration behavior of piezoceramic annular disks in resonance. The advantage of using the AF-ESPI method is that both resonant frequencies and the corresponding full-field mode shapes can be obtained simultaneously from the experimental measurement. The fringe patterns shown in the experimental results correspond directly to the vibrating mode shapes. The experimental results obtained from the impedance analyzer and the theoretical predictions show that only the radial extensional vibration for the piezoceramic annular disk can be measured by the impedance analysis. However, both the transverse and extensional vibration modes and resonant frequencies can be obtained by the AF-ESPI technique. In addition to the AF-ESPI technique, the transverse vibration frequency is measured and verified by the LDV system. Commercially available finite-element analysis software also is used to provide the numerical solutions of resonant frequencies and mode shapes. Good agreements of the mode shapes and resonant frequencies are obtained for the experimental and theoretical results. To understand the influences of the inner-to-outer radius ratio on the vibration characteristics, the dependence of resonant frequencies and dynamic electromechanical coupling coefficients on the inner-to-outer radius ratio also is presented in this work.

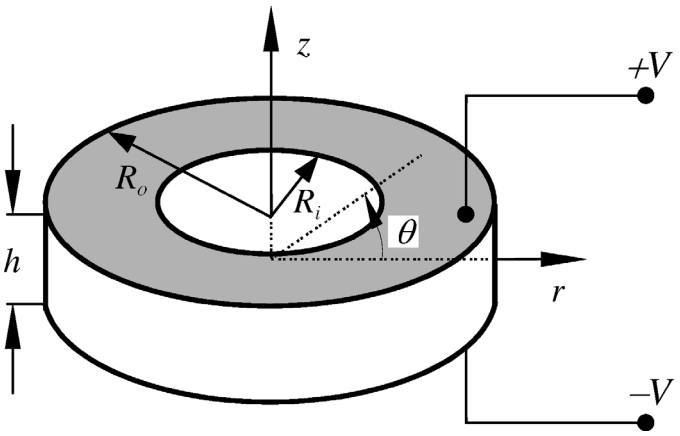

Fig. 1. Geometry and coordinate system of the piezoceramic annular disk.

II. Formulations and Theoretical Results of Piezoceramic Annular Disks

Fig. 1 shows the geometric configuration of piezoceramic annular disk with external radius R_0, internal radius R_i, and thickness h. The annular disk is assumed to be thin, $h \ll R_i$. The cylindrical coordinate system is adopted where the $r-\theta$ plane is coincident with the mid-plane of the undeformed annular disk, and the origin is in the center of the disk. The piezoceramic annular disk is polarized in the thickness direction, and two opposite surfaces are fully covered by electrodes. For the theoretical analysis, the system of governing equations and basic hypotheses used in this study to determine the vibration characteristics of a piezoceramic annular disk are presented following Rogacheva [19]. The differential equations of equilibrium

for three-dimensional problems in cylindrical coordinates are:

$$\frac{\partial \sigma_{rr}}{\partial r}+\frac{1}{r}\frac{\partial \sigma_{r\theta}}{\partial \theta}+\frac{\partial \sigma_{rz}}{\partial z}+\frac{1}{r}\left(\sigma_{rr}-\sigma_{\theta\theta}\right)+\rho\frac{\partial^2 u}{\partial t^2}=0, \tag{1a}$$

$$\frac{\partial \sigma_{r\theta}}{\partial r}+\frac{1}{r}\frac{\partial \sigma_{\theta\theta}}{\partial \theta}+\frac{\partial \sigma_{\theta z}}{\partial z}+\frac{2}{r}\sigma_{r\theta}+\rho\frac{\partial^2 v}{\partial t^2}=0, \tag{1b}$$

$$\frac{\partial \sigma_{rz}}{\partial r}+\frac{1}{r}\frac{\partial \sigma_{\theta z}}{\partial \theta}+\frac{\partial \sigma_{zz}}{\partial z}+\frac{1}{r}\sigma_{rz}+\rho\frac{\partial^2 w}{\partial t^2}=0, \tag{1c}$$

where $\sigma_{rr}, \sigma_{r\theta}, \ldots, \sigma_{zz}$ are the components of the stress tensor; $u(r,\theta,z,t)$, $v(r,\theta,z,t)$ and $w(r,\theta,z,t)$ are the displacements of the disk in the radial, tangential, and transverse direction, respectively; and ρ is the material density. The strain-mechanical displacement relations for three-dimensional problems in cylindrical coordinates are given by:

$$\begin{aligned} e_{rr}&=\frac{\partial u}{\partial r},\quad e_{\theta\theta}=\frac{u}{r}+\frac{1}{r}\frac{\partial v}{\partial \theta},\\ e_{zz}&=\frac{\partial w}{\partial z},\quad e_{r\theta}=\frac{1}{r}\frac{\partial u}{\partial \theta}+\frac{\partial v}{\partial r}-\frac{v}{r},\\ e_{rz}&=\frac{\partial u}{\partial z}+\frac{\partial w}{\partial r},\quad e_{\theta z}=\frac{\partial v}{\partial z}+\frac{1}{r}\frac{\partial w}{\partial \theta}, \end{aligned} \tag{2}$$

where $e_{rr}, e_{r\theta}, \ldots, e_{zz}$ are the components of the infinitesimal strain and are functions of r, θ, z, and t. The linear constitutive equations for a piezoceramic material with crystal symmetry class C_{6mm} are:

$$\begin{bmatrix} e_{rr}\\ e_{\theta\theta}\\ e_{zz}\\ e_{\theta z}\\ e_{rz}\\ e_{r\theta}\\ D_r\\ D_\theta\\ D_z \end{bmatrix} = \begin{bmatrix} s_{11}^E & s_{12}^E & s_{13}^E & 0 & 0 & 0 & 0 & 0 & d_{31}\\ s_{12}^E & s_{11}^E & s_{13}^E & 0 & 0 & 0 & 0 & 0 & d_{31}\\ s_{13}^E & s_{13}^E & s_{33}^E & 0 & 0 & 0 & 0 & 0 & d_{33}\\ 0 & 0 & 0 & s_{44}^E & 0 & 0 & 0 & d_{15} & 0\\ 0 & 0 & 0 & 0 & s_{44}^E & 0 & d_{15} & 0 & 0\\ 0 & 0 & 0 & 0 & 0 & s_{66}^E & 0 & 0 & 0\\ 0 & 0 & 0 & 0 & d_{15} & 0 & \varepsilon_{11}^T & 0 & 0\\ 0 & 0 & 0 & d_{15} & 0 & 0 & 0 & \varepsilon_{11}^T & 0\\ d_{31} & d_{31} & d_{33} & 0 & 0 & 0 & 0 & 0 & \varepsilon_{33}^T \end{bmatrix} \begin{bmatrix} \sigma_{rr}\\ \sigma_{\theta\theta}\\ \sigma_{zz}\\ \sigma_{\theta z}\\ \sigma_{rz}\\ \sigma_{r\theta}\\ E_r\\ E_\theta\\ E_z \end{bmatrix}, \tag{3}$$

where $s_{11}^E, s_{12}^E, \ldots, s_{66}^E$ are the compliance constants; d_{15}, d_{31}, d_{33} are the piezoelectric constants; $\varepsilon_{11}^T, \varepsilon_{33}^T$ are the dielectric constants; D_r, D_θ, D_z are the components of the electrical displacement; and E_r, E_θ, E_z are the components of the electrical field. The piezoceramic material is isotropic in the plane normal to the z-axis. The charge equation of electrostatics is represented as:

$$\frac{\partial D_r}{\partial r}+\frac{1}{r}\frac{\partial D_\theta}{\partial \theta}+\frac{1}{r}D_r+\frac{\partial D_z}{\partial z}=0. \tag{4}$$

The electric field-electric potential relations are given by:

$$E_r=-\frac{\partial \varphi}{\partial r},\quad E_\theta=-\frac{1}{r}\frac{\partial \varphi}{\partial \theta},\quad E_z=-\frac{\partial \varphi}{\partial z}, \tag{5}$$

where φ is the electrical potential. Because the piezoceramic annular disk is thin and the deformation is small, some hypotheses to simplify the theoretical analysis are indicated as follows:

- Normal stress σ_{zz} is very small and can be neglected relative to the other stresses, we set $\sigma_{zz}=0$.
- The rectilinear element normal to the middle surface before deformation remains perpendicular to the strained surface after deformation, and its elongation can be neglected, i.e., $e_{rz}=e_{\theta z}=0$.
- Electrical potential varies with the thickness of the piezoceramic annular disk by the square law, i.e., $\varphi(r,\theta,z,t)=\varphi_0(r,\theta,t)+z\varphi_1(r,\theta,t)+z^2\varphi_2(r,\theta,t)$; where φ_0, φ_1, and φ_2 are unknown electric potential parameters.
- Electrical displacement D_z is a constant with respect to the thickness.

According to the first hypothesis, the electroelasticity relation of (3) can be simplified as:

$$\sigma_{rr}=\frac{1}{s_{11}^E\left(1-v_p^2\right)}\left(e_{rr}+v_p e_{\theta\theta}\right)-\frac{d_{31}}{s_{11}^E\left(1-v_p\right)}E_z, \tag{6a}$$

$$\sigma_{\theta\theta}=\frac{1}{s_{11}^E\left(1-v_p^2\right)}\left(e_{\theta\theta}+v_p e_{rr}\right)-\frac{d_{31}}{s_{11}^E\left(1-v_p\right)}E_z, \tag{6b}$$

$$\sigma_{r\theta}=\frac{1}{s_{66}^E}e_{r\theta}=\frac{e_{r\theta}}{2s_{11}^E\left(1+v_p\right)}, \tag{6c}$$

$$D_z=d_{31}\left(\sigma_{rr}+\sigma_{\theta\theta}\right)+\varepsilon_{33}^T E_z, \tag{6d}$$

where $v_p=-\frac{s_{12}^E}{s_{11}^E}$ is the planar Poisson's ratio. From the second hypothesis, the displacement fields for the first-order, shear-deformation theory (or Mindlin's plate theory) can be expressed as:

$$\begin{aligned} u(r,\theta,z,t)&=u_r(r,\theta,t)+z\frac{\partial w_z(r,\theta,t)}{\partial r},\\ v(r,\theta,z,t)&=v_\theta(r,\theta,t)+\frac{z}{r}\frac{\partial w_z(r,\theta,t)}{\partial \theta},\\ w(r,\theta,z,t)&=w_z(r,\theta,t). \end{aligned}$$

It is noted that $u_r=u\big|_{z=0}$, $v_\theta=v\big|_{z=0}$ and $w_z=w\big|_{z=0}$ represent the radial, the tangential, and the transverse displacements of the middle surface of the plate, respectively. The strain-mechanical displacement relations presented in (2) can be rewritten as:

$$e_{rr}=\frac{\partial u_r}{\partial r}+z\frac{\partial^2 w_z}{\partial r^2}, \tag{7a}$$

$$e_{\theta\theta}=\frac{u_r}{r}+\frac{1}{r}\frac{\partial v_\theta}{\partial \theta}+\frac{z}{r}\left[\frac{\partial w_z}{\partial r}+\frac{\partial}{\partial \theta}\left(\frac{1}{r}\frac{\partial w_z}{\partial \theta}\right)\right], \tag{7b}$$

$$\begin{aligned} e_{r\theta}=&\frac{1}{r}\frac{\partial u_r}{\partial \theta}+\frac{z}{r}\frac{\partial^2 w_z}{\partial r\partial \theta}+\frac{\partial v_\theta}{\partial r}\\ &+z\frac{\partial}{\partial r}\left(\frac{1}{r}\frac{\partial w_z}{\partial \theta}\right)-\frac{v_\theta}{r}-\frac{z}{r^2}\frac{\partial w_z}{\partial \theta}. \end{aligned} \tag{7c}$$

From the above-mentioned assumptions, the original three-dimensional problem is reduced to a two-dimensional problem. Because the piezoceramic annular plate is thin, the out-of-plane (transverse) vibration and the in-plane (tangential and extensional) vibration are assumed to be

decoupled. We will analyze in detail the dynamic characteristics for transverse, tangential, and extensional vibrations, including the resonant frequencies, mode shapes, and electrical currents. The nonaxisymmetric modes are investigated for transverse vibration, and the tangential and extensional vibrations are restricted to axisymmetric modes.

A. Transverse Vibration

Suppose that the piezoceramic annular disk is driven by an alternative current (AC) voltage $Ve^{i\omega t}$ and the transverse vibration is nonaxisymmetric, the displacement in the z-direction can be assumed to have the following form:

$$w_z(r,\theta,t) = W(r,\theta)e^{i\omega t}, \tag{8}$$

where ω is the angular frequency. If the time-dependent term $e^{i\omega t}$ is uniformly suppressed in the analysis, by substituting (8) into (7a)–(7c) and setting $u_r = v_\theta = 0$, then stress components in (6a)–(6c) can be expressed as:

$$\sigma_{rr} = \frac{1}{s_{11}^E\left(1-v_p^2\right)}\left[z\frac{\partial^2 W}{\partial r^2} + v_p\frac{z}{r}\left(\frac{\partial W}{\partial r} + \frac{1}{r}\frac{\partial^2 W}{\partial \theta^2}\right)\right] - \frac{d_{31}}{s_{11}^E\left(1-v_p\right)}E_z, \tag{9a}$$

$$\sigma_{\theta\theta} = \frac{1}{s_{11}^E\left(1-v_p^2\right)}\left[\frac{z}{r}\left(\frac{\partial W}{\partial r} + \frac{1}{r}\frac{\partial^2 W}{\partial \theta^2}\right) + v_p z\frac{\partial^2 W}{\partial r^2}\right] - \frac{d_{31}}{s_{11}^E\left(1-v_p\right)}E_z, \tag{9b}$$

$$\sigma_{r\theta} = \frac{1}{s_{11}^E\left(1+v_p\right)}\left[\frac{z}{r}\frac{\partial^2 W}{\partial r\partial\theta} - \frac{z}{r^2}\frac{\partial W}{\partial\theta}\right]. \tag{9c}$$

Herein it is assumed that the stresses as indicated in (9a)–(9c) are induced by the out-of-plane displacement $W(r,\theta)$ only. The electrical potential boundary condition on two electrode surfaces is:

$$\varphi\big|_{z=\pm\frac{h}{2}} = \pm V. \tag{10}$$

From (5), (9a), (9b), (10), and the third and fourth hypotheses, the electrical field can be represented as:

$$E_z = -\frac{2V}{h} - \frac{d_{31}}{\varepsilon_{33}^T}\frac{z}{s_{11}^E\left(1-v_p\right)\left(1-k_p^2\right)} \cdot \left[\frac{\partial^2 W}{\partial r^2} + \frac{1}{r}\left(\frac{\partial W}{\partial r} + \frac{1}{r}\frac{\partial^2 W}{\partial\theta^2}\right)\right], \tag{11}$$

where $k_p = \sqrt{\frac{2d_{31}^2}{\varepsilon_{33}^T s_{11}^E(1-v_p)}}$ is the planar electromechanical coupling coefficient.

Applying the integral operator $\int_{-h/2}^{h/2}\ldots dz$ to the equilibrium equations (1a)–(1c), and using (9a)–(9c) and (11) yields the governing equation of the transverse vibration as:

$$D'\nabla^4 W - \rho h\omega^2 W = 0, \tag{12}$$

where ∇^4 is a biharmonic operator and in polar coordinate system given by:

$$\nabla^4 = \left(\frac{\partial^2}{\partial r^2} + \frac{1}{r}\frac{\partial}{\partial r} + \frac{1}{r^2}\frac{\partial^2}{\partial\theta^2}\right)\left(\frac{\partial^2}{\partial r^2} + \frac{1}{r}\frac{\partial}{\partial r} + \frac{1}{r^2}\frac{\partial^2}{\partial\theta^2}\right).$$

The equivalent bending stiffness is defined by:

$$D' = \frac{h^3}{12}\cdot\frac{2-\left(1-v_p\right)k_p^2}{2s_{11}^E\left(1-v_p^2\right)\left(1-k_p^2\right)}. \tag{13}$$

According to (12), the general solution of the nonaxisymmetric transverse vibration for the piezoceramic annular disk is:

$$W(r,\theta) = \left[C_1^{(n)}J_n(\beta_1 r) + C_2^{(n)}Y_n(\beta_1 r) + C_3^{(n)}I_n(\beta_1 r) + C_4^{(n)}K_n(\beta_1 r)\right]\cos n\theta, \quad n = 0,1,2,3,\ldots, \tag{14a}$$

in which $C_1^{(n)} \sim C_4^{(n)}$ are constants and:

$$\beta_1^4 = \frac{\rho h\omega^2}{D'} = \frac{12\rho\omega^2}{h^2}\cdot\frac{2s_{11}^E\left(1-v_p^2\right)\left(1-k_p^2\right)}{2-\left(1-v_p\right)k_p^2}. \tag{14b}$$

In (14a), J_n and Y_n are Bessel functions of the first and second kinds, respectively, and I_n and K_n are modified Bessel functions of the first and second kinds, respectively. The constants $C_1^{(n)}$, $C_2^{(n)}$, $C_3^{(n)}$, and $C_4^{(n)}$ can be determined by satisfying the stress-free boundary conditions at $r = R_i$ and $r = R_0$, we have:

$$\int_{-h/2}^{h/2} z\sigma_{rr}dz = 0, \tag{15a}$$

and:

$$\int_{-h/2}^{h/2}\sigma_{rz}dz + \frac{1}{r}\frac{\partial}{\partial\theta}\int_{-h/2}^{h/2} z\sigma_{r\theta}dz = 0. \tag{15b}$$

From (15a) and (15b), four systems of linear equations are obtained as follows:

$$[A]\cdot[C] = [F], \tag{16a}$$

where $[C] = [C_1^{(n)}, C_2^{(n)}, C_3^{(n)}, C_4^{(n)}]^T$, $[A]$ is a 4×4 square matrix and $[F]$ is a 4×1 zero matrix. The elements of the matrix $[A]$ are explicitly expressed as:

$$
\begin{aligned}
A_{11} &= G\alpha\xi \cdot J_{n+1}(\alpha\xi) + \left[Gn(n-1) - H(\alpha\xi)^2\right] \cdot J_n(\alpha\xi),\\
A_{12} &= G\alpha\xi \cdot Y_{n+1}(\alpha\xi) + \left[Gn(n-1) - H(\alpha\xi)^2\right] \cdot Y_n(\alpha\xi),\\
A_{13} &= -G\alpha\xi \cdot I_{n+1}(\alpha\xi) + \left[Gn(n-1) + H(\alpha\xi)^2\right] \cdot I_n(\alpha\xi),\\
A_{14} &= G\alpha\xi \cdot K_{n+1}(\alpha\xi) + \left[Gn(n-1) + H(\alpha\xi)^2\right] \cdot K_n(\alpha\xi),\\
A_{21} &= G\xi \cdot J_{n+1}(\xi) + \left[Gn(n-1) - H\xi^2\right] \cdot J_n(\xi),\\
A_{22} &= G\xi \cdot Y_{n+1}(\xi) + \left[Gn(n-1) - H\xi^2\right] \cdot Y_n(\xi),\\
A_{23} &= -G\xi \cdot I_{n+1}(\xi) + \left[Gn(n-1) + H\xi^2\right] \cdot I_n(\xi),\\
A_{24} &= G\xi \cdot K_{n+1}(\xi) + \left[Gn(n-1) + H\xi^2\right] \cdot K_n(\xi),\\
A_{31} &= \left[H(\alpha\xi)^3 + G\alpha\xi n^2\right] \cdot J_{n+1}(\alpha\xi)\\
&\quad - \left[H(\alpha\xi)^2 n + Gn^2(n-1)\right] \cdot J_n(\alpha\xi),\\
A_{32} &= \left[H(\alpha\xi)^3 + G\alpha\xi n^2\right] \cdot Y_{n+1}(\alpha\xi)\\
&\quad - \left[H(\alpha\xi)^2 n + Gn^2(n-1)\right] \cdot Y_n(\alpha\xi),\\
A_{33} &= \left[H(\alpha\xi)^3 - G\alpha\xi n^2\right] \cdot I_{n+1}(\alpha\xi)\\
&\quad + \left[H(\alpha\xi)^2 n - Gn^2(n-1)\right] \cdot I_n(\alpha\xi),\\
A_{34} &= \left[-H(\alpha\xi)^3 + G\alpha\xi n^2\right] \cdot K_{n+1}(\alpha\xi)\\
&\quad + \left[H(\alpha\xi)^2 n - Gn^2(n-1)\right] \cdot K_n(\alpha\xi),\\
A_{41} &= \left[H\xi^3 + G\xi n^2\right] \cdot J_{n+1}(\xi) - \left[H\xi^2 n + Gn^2(n-1)\right]\\
&\quad \cdot J_n(\xi),\\
A_{42} &= \left[H\xi^3 + G\xi n^2\right] \cdot Y_{n+1}(\xi) - \left[H\xi^2 n + Gn^2(n-1)\right]\\
&\quad \cdot Y_n(\xi),\\
A_{43} &= \left[H\xi^3 - G\xi n^2\right] \cdot I_{n+1}(\xi) + \left[H\xi^2 n - Gn^2(n-1)\right]\\
&\quad \cdot I_n(\xi),\\
A_{44} &= \left[-H\xi^3 + G\xi n^2\right] \cdot K_{n+1}(\xi) + \left[H\xi^2 n - Gn^2(n-1)\right]\\
&\quad \cdot K_n(\xi),
\end{aligned}
\tag{16b}
$$

in which

$$
\begin{aligned}
H &= \frac{1}{1+v_p} + \frac{k_p^2}{2\left(1-k_p^2\right)},\\
G &= \frac{1-v_p}{1+v_p},\\
\alpha &= \frac{R_i}{R_o}, \text{ and}\\
\xi &= \beta_1 R_o.
\end{aligned}
\tag{17}
$$

To obtain nontrivial solutions for the constants $C_1^{(n)} - C_4^{(n)}$, the determinant of the coefficient matrix $[A]$ must be equal to zero, and that will yield the characteristic equation of resonant frequencies for nonaxisymmetric transverse vibrations as:

$$\det[A] = 0. \tag{18}$$

It is noted that the value n in (18) denotes the number of nodal diameters, and the sequence of roots represents the number of nodal circles. From (14b), (17) and (18), we can obtain the transverse resonant frequencies of nonaxisymmetric modes for piezoceramic annular disks with traction-free boundary conditions on the inner and outer circles as:

$$f = \frac{\xi^2 h}{2\pi R_o^2}\sqrt{\frac{2-(1-v_p)\,k_p^2}{24\rho s_{11}^E\left(1-v_p^2\right)\left(1-k_p^2\right)}}. \tag{19}$$

From (6d), the electrical current I can be expressed as:

$$
\begin{aligned}
I &= \frac{\partial}{\partial t}\iint_S D_z ds\\
&= i\omega\int_0^{2\pi}\int_{R_i}^{R_b}\left\{\frac{d_{31}\,(1+v_p)\,z}{s_{11}^E\left(1-v_p^2\right)}\left[\frac{\partial^2 W}{\partial r^2} + \frac{1}{r}\frac{\partial W}{\partial r} + \frac{1}{r^2}\frac{\partial^2 W}{\partial\theta^2}\right]\right.\\
&\quad \left. + \left[\varepsilon_{33}^T - \frac{2d_{31}^2}{s_{11}^E\,(1-v_p)}\right]E_z\right\} r\,dr\,d\theta\\
&= i\omega\frac{2\pi V\varepsilon_{33}^T\left(k_p^2-1\right)}{h}\cdot R_o^2\left(1-\alpha^2\right).
\end{aligned}
\tag{20}
$$

It is noted that the integration in (20) can be worked out and expressed in a very simple form. As seen in (20), the electrical current I does not approach infinity, even if the transverse vibrations are excited at resonant frequencies. This implies that the resonant frequencies of transverse vibrations cannot be measured by the impedance variation method, such as an impedance analyzer.

B. Tangential Vibration

It is assumed that the motion of the tangential vibration is axisymmetric, the tangential displacement can be expressed as the form:

$$v_\theta(r,t) = \Theta(r)e^{i\omega t}. \tag{21}$$

Following the similar procedure, after suppressing the time-dependent term $e^{i\omega t}$, we have the stress components for the tangential vibration as:

$$\sigma_{rr} = \sigma_{\theta\theta} = -\frac{d_{31}}{s_{11}^E\,(1-v_p)}E_z, \tag{22a}$$

$$\sigma_{r\theta} = \frac{1}{2s_{11}^E\,(1+v_p)}\left[\frac{d\Theta}{dr} - \frac{\Theta}{r}\right], \tag{22b}$$

where:

$$E_z = -\frac{2V}{h}. \tag{22c}$$

Substituting (22) into the equilibrium equation (1b) and integrating over the thickness of piezoceramic annular disks yields the governing equation of the tangential vibration as:

$$\nabla^2\Theta - 2\rho\omega^2 s_{11}^E\,(1+v_p)\,\Theta = 0. \tag{23}$$

Eq. (23) can be solved, and the general solution of the tangential vibration is:

$$\Theta(r) = C_5 J_1(\beta_2 r) + C_6 Y_1(\beta_2 r), \tag{24a}$$

in which C_5 and C_6 are constants and:

$$\beta_2^2 = 2\rho s_{11}^E\,(1+v_p)\,\omega^2. \tag{24b}$$

With the aid of the boundary condition at $r = R_i$ and $r = R_o$:

$$\int_{-h/2}^{h/2} \sigma_{r\theta} dz = 0. \tag{25}$$

The characteristic equation of resonant frequencies for tangential vibrations is obtained as follows:

$$\begin{aligned}&[\alpha\zeta J_0(\alpha\zeta) - 2J_1(\alpha\zeta)] \cdot [\zeta Y_0(\zeta) - 2Y_1(\zeta)] \\ &\quad = [\alpha\zeta Y_0(\alpha\zeta) - 2Y_1(\alpha\zeta)] \cdot [\zeta J_0(\zeta) - 2J_1(\zeta)], \\ &\qquad\qquad \zeta = \beta_2 R_o. \end{aligned} \tag{26}$$

By solving the roots of (26) for ζ, the tangential resonant frequency for piezoceramic annular disks is:

$$f = \frac{\zeta}{2\pi R_o} \sqrt{\frac{1}{2\rho s_{11}^E (1 + v_p)}}. \tag{27}$$

The electrical current I for tangential vibrations can be worked out as:

$$\begin{aligned} I &= \frac{\partial}{\partial t} \iint_S D_z ds \\ &= i\omega \int_0^{2\pi} \int_{R_i}^{R_b} \left\{ \left[-\frac{2d_{31}^2}{s_{11}^E (1 - v_p)} + \varepsilon_{33}^T \right] E_z \right\} r dr d\theta \\ &= i\omega \frac{2\pi V \varepsilon_{33}^T \left(k_p^2 - 1\right)}{h} \cdot R_o^2 \left(1 - \alpha^2\right). \end{aligned} \tag{28}$$

It is clearly indicated in (28) that the resonant frequencies of tangential vibrations cannot be measured by the impedance variation method.

C. Extensional Vibration

Suppose that the extensional vibration is axisymmetric, the radial extensional displacement of the middle plane can be assumed to have the form:

$$u_r(r, t) = U(r) e^{i\omega t}. \tag{29}$$

The stress-displacement relations for the extensional vibration are given by:

$$\begin{aligned} \sigma_{rr} &= \frac{1}{s_{11}^E \left(1 - v_p^2\right)} \left[\frac{dU}{dr} + v_p \frac{U}{r} \right] \\ &\quad + \frac{d_{31}}{s_{11}^E (1 - v_p)} \cdot \frac{2V}{h}, \end{aligned} \tag{30a}$$

$$\begin{aligned} \sigma_{\theta\theta} &= \frac{1}{s_{11}^E \left(1 - v_p^2\right)} \left[\frac{U}{r} + v_p \frac{dU}{dr} \right] \\ &\quad + \frac{d_{31}}{s_{11}^E (1 - v_p)} \cdot \frac{2V}{h}, \end{aligned} \tag{30b}$$

in which (22c) has been used. Substituting (30) into the equilibrium equation (1a) and integrating over the thickness of plates, we have the governing equation of displacement for extensional vibrations:

$$\nabla^2 U - \rho\omega^2 s_{11}^E \left(1 - v_p^2\right) U = 0. \tag{31}$$

The general solution of (31) is:

$$U(r) = C_7 J_1(\beta_3 r) + C_8 Y_1(\beta_3 r), \tag{32a}$$

where C_7 and C_8 are constants and

$$\beta_3^2 = \rho s_{11}^E \left(1 - v_p^2\right) \omega^2. \tag{32b}$$

From the boundary conditions at $r = R_i$ and $r = R_o$, we have:

$$\int_{-h/2}^{h/2} \sigma_{rr} dz = 0. \tag{33}$$

The constants C_7 and C_8 are found in (34) (see next page), and $\eta = \beta_3 R_o$.

The electrical current I for extensional vibrations can be expressed as:

$$\begin{aligned} I &= \frac{\partial}{\partial t} \iint_S D_z ds = i\omega \int_0^{2\pi} \int_{R_i}^{R_b} \left\{ \frac{d_{31} (1 - v_p)}{s_{11}^E \left(1 - v_p^2\right)} \left[\frac{dU}{dr} + \frac{U}{r} \right] \right. \\ &\qquad \left. + \frac{2\varepsilon_{33}^T V}{h} \left(k_p^2 - 1\right) \right\} r dr d\theta \\ &= i\omega \frac{2\pi R_o^2 V \varepsilon_{33}^T}{h} \cdot \frac{(1 + v_p) k_p^2 \Delta_2 + \left(k_p^2 - 1\right) \left(1 - \alpha^2\right) \Delta_1}{\Delta_1}, \end{aligned} \tag{35a}$$

where:

$$\begin{aligned} \Delta_2 &= \alpha\eta [J_0(\eta) - J_0(\alpha\eta)] \cdot [Y_1(\eta) - \alpha Y_1(\alpha\eta)] \\ &\quad - \alpha\eta [Y_0(\eta) - Y_0(\alpha\eta)] \cdot [J_1(\eta) - \alpha J_1(\alpha\eta)] \\ &\quad + \left(1 - \alpha^2\right) (1 - v_p) [J_1(\alpha\eta) Y_1(\eta) - J_1(\eta) Y_1(\alpha\eta)]. \end{aligned} \tag{35b}$$

From (35a), the resonant frequencies can be determined when the current I approaches infinity. We readily obtain the characteristic equations of resonant frequencies and antiresonant frequencies for extensional vibrations as:

$$\Delta_1 = 0, \tag{36a}$$

and

$$(1 + v_p) k_p^2 \Delta_2 + \left(k_p^2 - 1\right) \left(1 - \alpha^2\right) \Delta_1 = 0. \tag{36b}$$

From (36a) and (36b), the radial extensional resonant and antiresonant frequencies for piezoceramic annular disks with traction-free boundary conditions are expressed as:

$$f = \frac{\eta}{2\pi R_o} \sqrt{\frac{1}{\rho s_{11}^E \left(1 - v_p^2\right)}}. \tag{37}$$

III. Theory of the Time-Averaged AF-ESPI Method

The most familiar way of ESPI used for vibration analysis is the time-averaged method with an image sensor [the

$$C_7 = \frac{2Vd_{31}(1+v_p)R_o[\alpha\eta Y_0(\alpha\eta) - (1-v_p)Y_1(\alpha\eta) - \alpha\eta Y_0(\eta) + \alpha(1-v_p)Y_1(\eta)]}{\Delta_1 h}, \tag{34a}$$

$$C_8 = \frac{2Vd_{31}(1+v_p)R_o[-\alpha\eta J_0(\alpha\eta) + (1-v_p)J_1(\alpha\eta) + \alpha\eta J_0(\eta) - \alpha(1-v_p)J_1(\eta)]}{\Delta_1 h}, \tag{34b}$$

where:

$$\begin{aligned}\Delta_1 = {} & [\alpha\eta J_0(\alpha\eta) - (1-v_p)J_1(\alpha\eta)][\eta Y_0(\eta) - (1-v_p)Y_1(\eta)] \\ & - [\alpha\eta Y_0(\alpha\eta) - (1-v_p)Y_1(\alpha\eta)][\eta J_0(\eta) - (1-v_p)J_1(\eta)],\end{aligned} \tag{34c}$$

most commonly used is a charge-coupled device (CCD) array] integrating the speckle interferogram field pixel by pixel. The name "time-averaged" denotes that the vibration measurement includes many periods of object motions during the camera period. Two different optical setups are used for the vibration measurement in this study. For the out-of-plane, full-field vibration measurement using the AF-ESPI method, the first image is recorded as a reference after the specimen vibrates periodically. As the vibration of the specimen continues, the vibration amplitude changes from a to $a + \Delta a$ because of the electronic noise or instability of the apparatus. When the vibration amplitude variation Δa is small, subtract the first image from the second by the image processing system, and the resulting image intensity can be expressed as:

$$I = \frac{\sqrt{I_o I_r}}{2}\left|(\cos\Phi)\cdot\left[\frac{2\pi\Delta a}{\lambda}(1+\cos\Psi)\right]^2 \cdot J_0\left[\frac{2\pi a}{\lambda}(1+\cos\Psi)\right]\right|, \tag{38}$$

where I_o is the object light intensity, I_r is the reference light intensity, Φ is the phase difference between object and reference light, λ is the wavelength of laser, and Ψ is the angle between object light and observation direction.

Similar to the out-of-plane vibration case, we can obtain the resulting image intensity for the in-plane vibration measurement as:

$$I = \frac{I_o}{2}\left|(\cos\Phi')\cdot\left[\frac{2\pi\Delta a'}{\lambda}(2\sin\Psi')\right]^2 \cdot J_0\left[\frac{2\pi a'}{\lambda}(2\sin\Psi')\right]\right|, \tag{39}$$

where Φ' is the phase difference between two object lights, a' is the vibration amplitude of in-plane vibration, and Ψ' is half of the angle between two illumination lights.

From (38) and (39), we can see that the fringe patterns for both the out-of-plane and in-plane vibrations obtained by the AF-ESPI method are dominated by a zero-order Bessel function J_0. The AF-ESPI method for transverse vibration was first proposed by Wang *et al.* [20]. Ma and Huang [17] provided a detailed discussion of the AF-ESPI method to investigate both the out-of-plane and in-plane vibrations of piezoelectric rectangular parallelepipeds for a three-dimensional configuration. Combining the out-of-plane with in-plane optical setups by the AF-ESPI method, we can construct completely the vibration characteristics of the piezoceramic annular disks, including resonant frequencies and mode shapes at the same time. This is different from the conventional impedance analysis, which has been used widely in determining only the in-plane resonant frequencies for piezoceramic materials.

TABLE I
MATERIAL PROPERTIES OF PIEZOCERAMICS PIC-151.

PIC-151 ceramics	
s_{11}^E (10^{-12} m^2/N)	16.83
s_{33}^E	19.0
s_{12}^E	−5.656
s_{13}^E	−7.107
s_{44}^E	50.96
s_{66}^E	44.97
d_{31} (10^{-10} m/V)	−2.14
d_{33}	4.23
d_{15}	6.1
ε_{11}^T (10^{-9} F/m)	17.134
ε_{33}^T	18.665
ρ (kg/m^3)	7800

IV. THEORETICAL AND EXPERIMENTAL RESULTS

A piezoceramic annular disk with outer radius R_o = 15 mm, inner radius R_i = 7.5 mm, and thickness h = 1 mm is selected for experimental investigations; the modal number of the specimen is PIC-151 (Physik Instrumente, Lederhose, Germany). The polarization is in the z-direction, and two opposite faces of the specimen are completely coated by silver electrodes as shown in Fig. 1. The piezoceramic annular disk is excited by the application of an AC voltage across electrodes on the two surfaces and has completely stress-free boundary conditions. The electroelastic properties of the test specimen PIC-151 are listed in Table I. Analytically, boundary condition can be specified as completely free or any constrained situations. The completely free boundary means that the specimen is, in fact, floating in space with no attachment or connec-

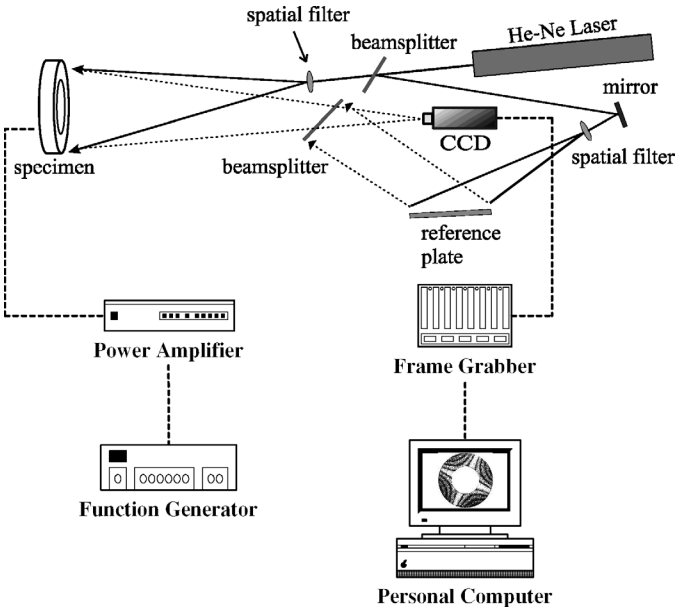

Fig. 2. Schematic of AF-ESPI setup for out-of-plane measurement.

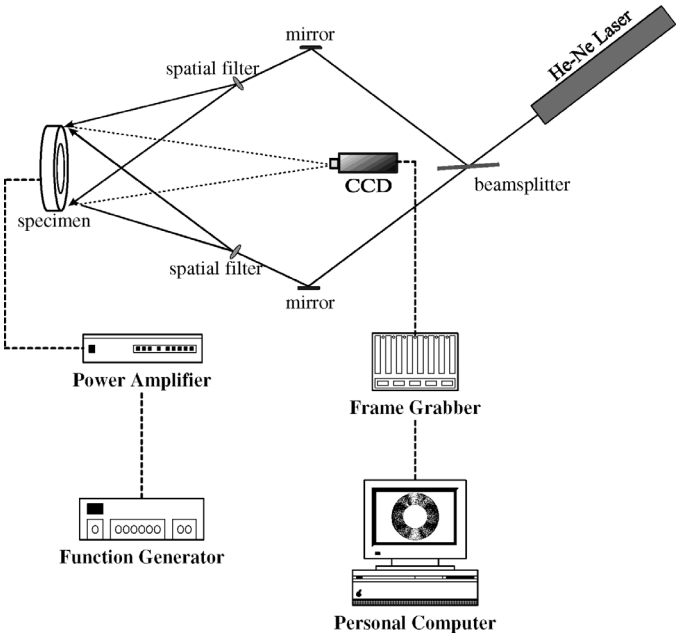

Fig. 3. Schematic of AF-ESPI setup for in-plane measurement.

tion in ground and exhibits rigid body behavior at zero frequency. In testing practice, however, it is almost not realizable and generally not possible to fully achieve this condition. Hence, the specimen must be supported in some manner to model the completely free boundary. In this study, to experimentally model the completely free boundary, the piezoceramic annular disk is placed on the surface of a very soft sponge with the dimensions $80 \times 60 \times 23$ mm and is stuck by a narrow adhesive tape on the surface of sponge.

The most common light source for ESPI is a continuous wave laser because of the lower price and optical power requirement. When the continuous wave laser is used, time-averaged interferometric fringes are produced for the harmonically vibrating object, which offers a good observation of the vibration mode shapes. The schematic layout of the self-arranged, time-averaged AF-ESPI optical systems as shown in Figs. 2 and 3 are used to perform the out-of-plane (transverse) and in-plane (extensional) experimental measurements for resonant frequencies and corresponding mode shapes. A continuous-wave He-Ne laser (25-LHP-928-249, Melles Griot, Carlsbad, CA) with the wavelength $\lambda = 632.8$ nm is used as the coherent light source. We use a CCD camera (Pulnix TM-7CN, Pulnix America, Inc., Sunnyvale, CA) and a frame grabber (Dipix P360F, Dipix Technologies Inc., Ottawa, ON, Canada) with a digital signal processor onboard to record and process the images obtained from interferogram of the object and reference beams. The interpretation of the fringe image is similar to the reading of a displacement contour. To achieve the sinusoidal output, a function generator (HP-33120A, Hewlett Packard, Palo Alto, CA) connected to a power amplifier (NF Electronic Instruments 4005 type, NF Corporation, Kohokuku, Yokohama, Japan) is used as an input source, which generates a periodical exciting force to the specimen.

Detailed experimental measurement procedure of the AF-ESPI technique is performed as follows. Once the specimen is excited into vibration, the interferogram recorded by the CCD camera is stored in an image buffer as a reference image, then the next image is grabbed and is subtracted by the image processing system. If the frequency of vibration is not the resonant frequency, only random distributed speckles are displayed and no fringe patterns will be shown in the monitor. However, if the frequency of vibration is in the neighborhood of the resonant frequency, stationary distinct fringe patterns will be observed in the monitor. Then, as the function generator is carefully and slowly adjusted, the number of fringes will increase and the fringe pattern will become more clear as the resonant frequency is approached. From the aforementioned experimental procedure, the resonant frequencies and the correspondent mode shapes can be determined at the same time.

From the AF-ESPI optical system and the experimental procedure mentioned above, the resonant frequencies and corresponding mode shapes for the transverse and extensional vibrations can be experimentally determined. In addition to the theoretical analysis and experimental measurement, finite-element calculation also is performed using the commercially available software ABAQUS finite-element package[1] in which 20-node, three-dimensional, solid piezoelectric elements (C3D20E, Hibbit, Karlsson, and Sorensen, Inc., Pawtucket, RI) are selected to analyze the problem. Fig. 4 shows the experimental and numerical results for the first six mode shapes of transverse vibrations, and Fig. 5 shows the first two mode shapes of extensional vibrations. In Figs. 4 and 5, we indicate the

[1]ABAQUS User's Manual, ver. 5.8., Pawtucket, RI: Hibbit, Karlsson, and Sorensen, Inc., 1998.

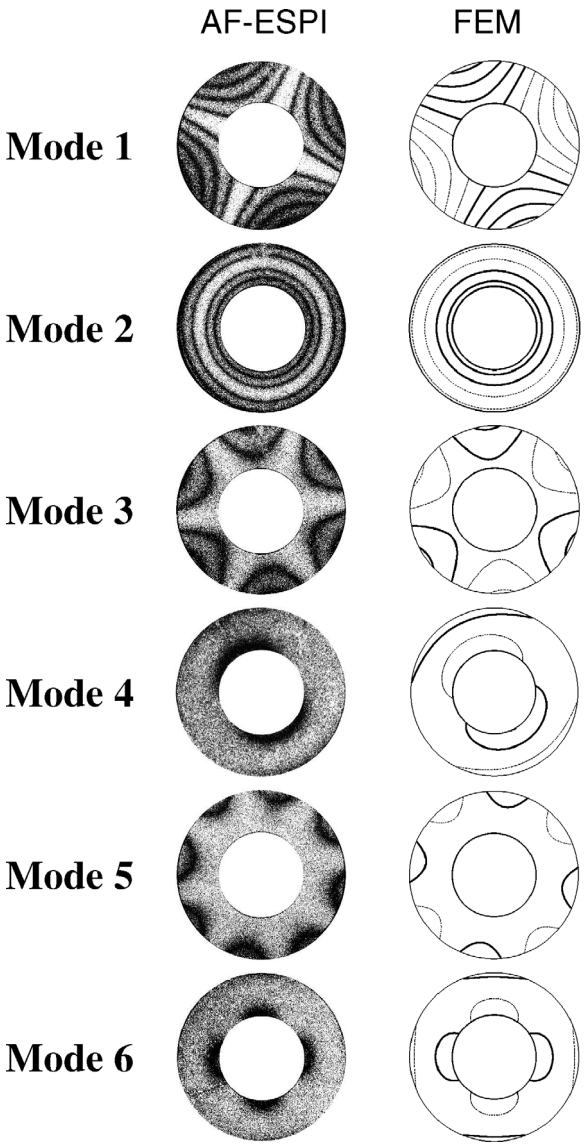

Fig. 4. Mode shapes of the transverse vibration obtained by AF-ESPI and FEM for the piezoceramic annular disk.

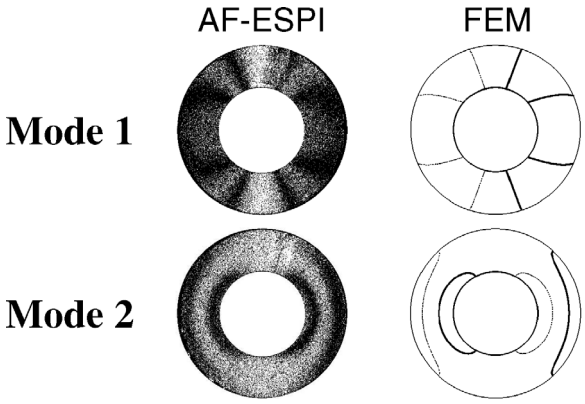

Fig. 5. Mode shapes of the extensional vibration obtained by AF-ESPI and FEM for the piezoceramic annular disk.

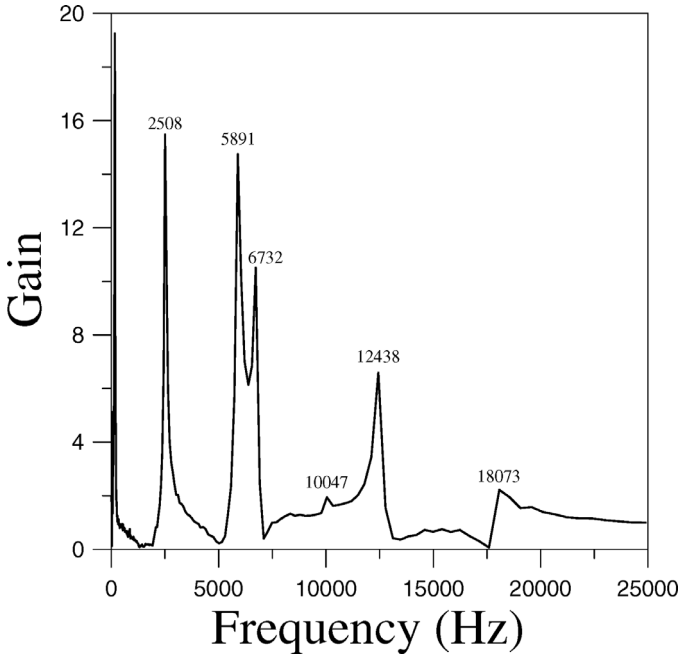

Fig. 6. LDV output gain spectrum of transverse vibrations for the piezoceramic annular disk.

phase of displacement in finite-element results as solid or dotted lines, with the solid lines in the opposite direction to the dotted lines. The transition from solid lines to dotted lines corresponds to a zero displacement line, or a nodal line. The zero-order fringe, which is the brightest fringe in experimental results, represents the nodal lines of the vibrating piezoceramic annular disk at resonance. The rest of the fringes are contours of constant amplitudes of displacement. The mode shapes obtained by experimental results can be checked by the nodal lines and fringe patterns with the numerical calculations. Excellent agreements between the experimental measurement and numerical calculation are found for both transverse and extensional vibration modes. We can see from Fig. 4 that the first three modes of the transverse vibration can be excited easily, and a relatively large amplitude of the displacement can be obtained. However, modes 4 and 6 cannot be excited easily, and very few fringe curves can be observed from the AF-ESPI optical system.

Herein a point-wise optical technique called the laser Doppler vibrometer (LDV) (AVID, Ahead Optoelectronics Inc., Chung-Ho, Taipei, Taiwan) also is used to validate the resonant frequencies of transverse vibration modes, and the gain spectrum is indicated in Fig. 6. The optical system for measuring dynamic displacements in the experiment is developed from the principle of the Michelson interferometer and the Doppler effect. For the LDV system, a built-in dynamic signal analyzer (DSA) composed of dynamic signal analyzer software and a plug-in waveform generator board can provide the specimen with the swept-sine excitation signal. In the analysis software, the swept-sine excitation signal is taken as input and the response measured by LDV is converted into the voltage signal and is taken as

TABLE II
RESULTS OF RESONANT FREQUENCIES OBTAINED BY THEORY, FEM, LDV, AND AF-ESPI OF THE TRANSVERSE VIBRATION.

Transverse mode	Theory (Hz)	FEM (Hz)	LDV (Hz)	AF-ESPI (Hz)	Error (a)(b)[1]	Difference (c)(d)[1]
1	2665	2626	2508	2500	1.52%	0.32%
2	6089	6028	5891	5900	1.01%	−0.15%
3	7169	7025	6732	6715	2.05%	0.25%
4	10816	10274	10047	10040	5.28%	0.07%
5	13282	12892	12438	12400	3.03%	0.31%
6	19878	18647	18073	18065	6.60%	0.04%

[1] (a) Theory, (b) FEM, (c) LDV, (d) AF-ESPI.

TABLE III
RESULTS OF RESONANT FREQUENCIES OBTAINED BY THEORY, FEM, IMPEDANCE ANALYSIS, AND AF-ESPI OF THE EXTENSIONAL VIBRATION.

Extensional mode	Theory (Hz)	FEM (Hz)	Impedance (Hz)	AF-ESPI (Hz)	Error (a)/(b)[2]	Difference (c)/(d)[2]
1	40741 (44597)[1]	40739 (44898)	40500 (43500)	40450	0.005% (−0.67%)	0.12%
2	200941 (233309)	200350 (242281)	207803 (234353)	207800	0.29% (−3.70%)	0.001%
3	393436 (394011)	388743 (463328)	399087 (411203)	—	1.21% (−14.96%)	—

[1] ( ) represents the antiresonant frequencies.
[2] (a) Theory, (b) FEM, (c) Impedance, (d) AF-ESPI.

output. After the fast Fourier transform (FFT) processing of the input and output with the DSA software, the ratio of output/input ("gain") is obtained. The result chart that shows the frequency response curve can be obtained. The peaks appearing in the frequency response curve are resonant frequencies for transverse vibrations. It also is shown in Fig. 6 that the gain of modes 4 and 6 are smaller than that of the other four modes, which agree with the above mentioned that modes 4 and 6 are difficult to excite. Table II shows the first six transverse resonant frequencies of the piezoceramic annular disk obtained by the AF-ESPI, LDV, theoretical prediction, and the finite-element calculation. It is worthy to note that the theoretical predictions [i.e., from (18) and (19)] agree well with the finite-element results, with the discrepancies within 6.6%. For the experimental measurements by AF-ESPI and LDV, the results are in excellent agreement with the differences below 0.4%. The comparison of the resonant frequencies obtained from the analytical method and experimental measurements are also in good agreement.

The electrical impedance of the piezoceramic material will drop to a local minimum when it vibrates at a resonant frequency. Hence, the resonant frequency also can be determined by the impedance analysis. Experimental impedance measurements of the piezoceramic annular disk are obtained by an impedance/gain-phase analyzer (HP-4194A, Hewlett Packard, Palo Alto, CA). The experimental result of the piezoceramic annular disk measured by HP-4194A and the simulated impedance curve calculated by (35a) are shown in Fig. 7. We can see that both results correlate well. The local minima and maxima appearing in the impedance curve correspond to the resonant and antiresonant frequencies, respectively. As we expected, only the resonant frequencies of the radial extensional modes are indicated in Fig. 7. Table III shows the first three extensional resonant frequencies of the piezoceramic annular disk obtained by the AF-ESPI, impedance analysis, theo-

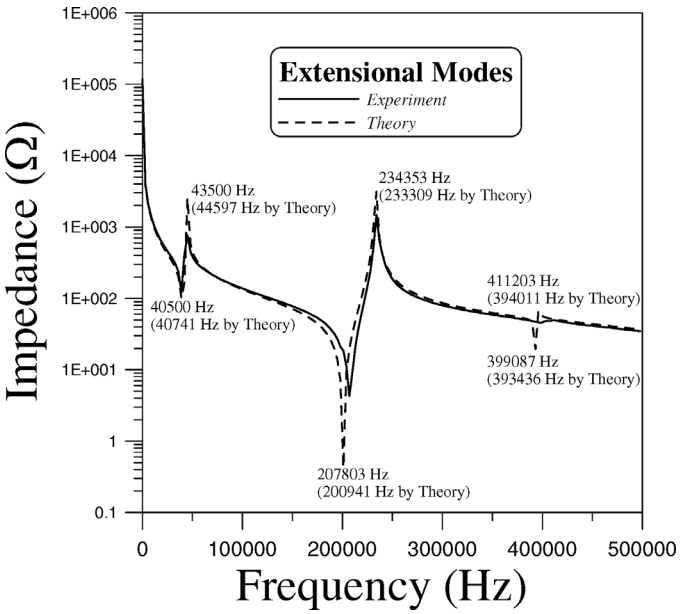

Fig. 7. Experimental and simulated impedance variation curves of the piezoceramic annular disk.

TABLE IV
RESULTS OF RESONANT FREQUENCIES OBTAINED BY THEORY AND FEM OF THE TANGENTIAL VIBRATION.

Tangential mode	Theory (Hz)	FEM (Hz)	Error
1	122067	122074	−0.006%
2	230301	230338	−0.016%
3	341195	341713	−0.15%

retical prediction, and the finite-element calculation. The third mode is very difficult to excite, and the amplitude of the vibration is beyond the sensitivity of the AF-ESPI method. Table III also shows the correspondent antiresonant frequencies obtained from impedance analysis, theoretical prediction, and finite element modeling (FEM). The discrepancy of resonant frequencies between AF-ESPI and impedance analysis is smaller than 0.2%. The difference between the experimental measurements and theoretical results may result from the determination of the material properties or the defects of the piezoceramic annular disks.

From the experimental techniques previously mentioned, we find that the tangential vibration modes cannot be obtained by the impedance analyzer. Hence, only the theoretical analysis and finite-element calculation are provided. Table IV shows the comparison between the theoretical predictions [i.e., from (26) and (27)] and FEM calculations for the first three tangential resonant frequencies of the piezoceramic annular disk. The discrepancies between the two results are within 0.06%.

With the aid of the characteristic equation of resonant frequencies for transverse vibrations, the variation in frequency parameter (ξ^2) for different inner-to-outer radius ratios (α) is shown in Fig. 8. As can be seen, the resonant frequencies approach those of a thin piezoceramic circular disk as $\alpha \to 0$. For further discussion, the transverse vibration modes are classified into two groups, named Group I and Group II in this article. Group I (modes 1, 3, 4, and 6 for $\alpha = 0$) has the pure nodal line along the radial direction, and Group II (modes 2, 5, and 7 for $\alpha = 0$) has at least one nodal line along the circular direction. The letters "n" and "s" in Fig. 8 indicate the number of nodal diameters and nodal circles of mode shapes for $\alpha = 0$, respectively. When the ratio α increases from zero to one for Group I, the resonant frequency has a maximum at $\alpha = 0$, then gradually decreases to a minimum at $\alpha = 1$. However, for Group II, the resonant frequency will decrease and reach a minimum ($\alpha = 0.34$ for mode 2, $\alpha = 0.49$ for mode 5, and $\alpha = 0.54$ for mode 7), then increases rapidly to infinity as $\alpha \to 1$. Hence, if the mode shape includes nodal circles, the resonant frequency will increase rapidly and approach infinity for $\alpha \to 1$ [or $(R_o - R_i) \to 0$)]. Subsequently, the mode shape for Group I will degenerate into the nodal points for $\alpha \to 1$ as is expected. In Fig. 8, we also find that the curves of resonant frequency for different modes will intersect at certain α values, meaning that the sequence of these modes is changed. For examples, modes 4 and 5 (modes 6 and 7) for $\alpha = 0$ will change the sequence

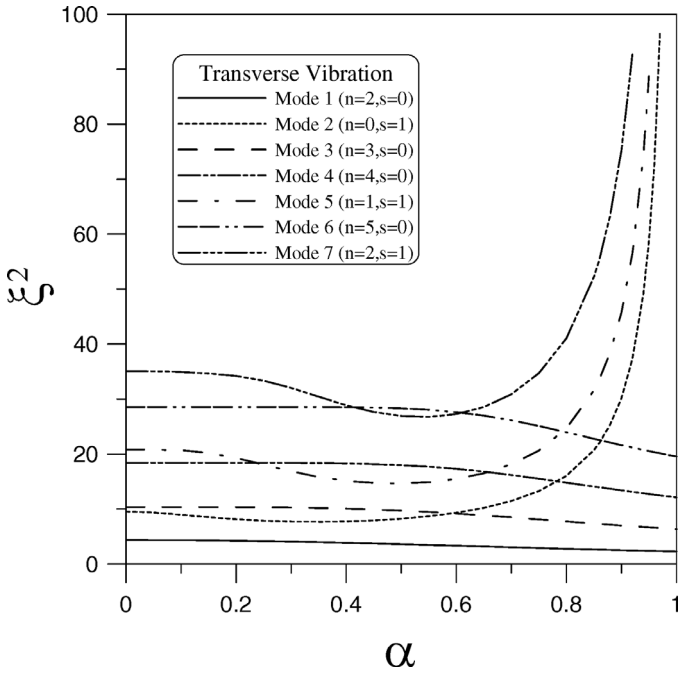

Fig. 8. The variation of frequency parameter of the transverse vibration for different values of α.

of the mode number for $\alpha = 0.5$. Figs. 9 and 10 show the variation in frequency parameter for tangential and extensional vibrations, respectively. For the tangential vibration mode as shown in Fig. 9, all the variations in resonant frequencies show the same trend, and they have the minimum value at $\alpha = 0$ and approach infinity as $\alpha \to 1$. Fig. 10 clearly shows that there are also two groups of vibration modes similar to the transverse vibration case. Only the first mode belongs to Group I, and Group II includes all the higher order vibration modes. The minimum value occurs at $\alpha = 0.2$ for mode 2 and $\alpha = 0.12$ for mode 3.

The electromechanical coupling coefficient is an important characteristic of piezoceramic elements that is frequently used to measure the energy conversion efficiency. The dynamic electromechanical coupling coefficient proposed by Mason [21] can be evaluated as:

$$k_d = \frac{\sqrt{f_a^2 - f_r^2}}{f_a}, \tag{40}$$

where f_r is the resonant frequency and f_a is the antiresonant frequency. Eq. (40) usually is used to determine the electromechanical coupling coefficient by measuring the resonant and antiresonant frequencies. The antiresonant frequency f_a is defined as the frequency with maximum resistance and can be evaluated by the condition that the electrical current I is zero. According to (36a) and (36b), the value of k_d is plotted as a function of α for the first three extensional modes, and the result is shown in Fig. 11. It is interesting to note that the value of k_d for the second mode increases when α increases, and the value of k_d for the first and third modes decreases when α increases. We note that mode 1 corresponds to an extensional vibration with R_o and R_i and vary in the same direction. It is not

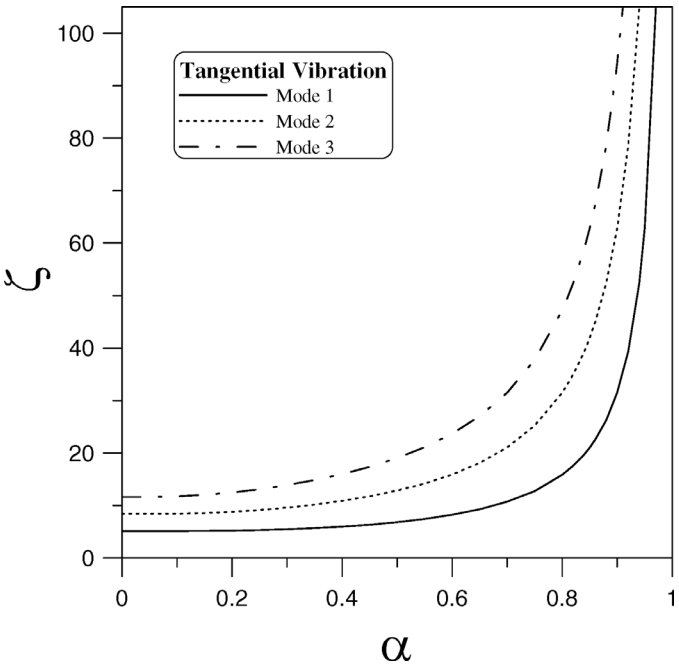

Fig. 9. The variation of frequency parameter of the tangential vibration for different values of α.

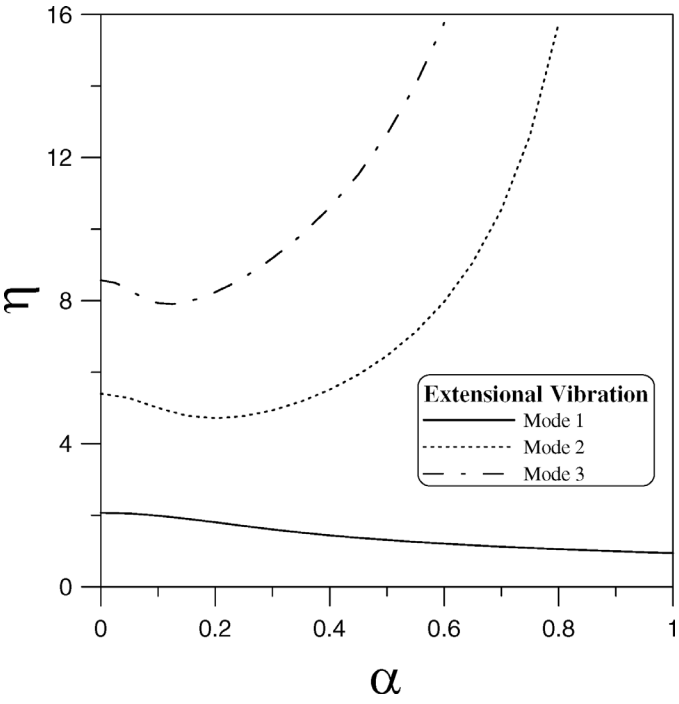

Fig. 10. The variation of frequency parameter of the extensional vibration for different values of α.

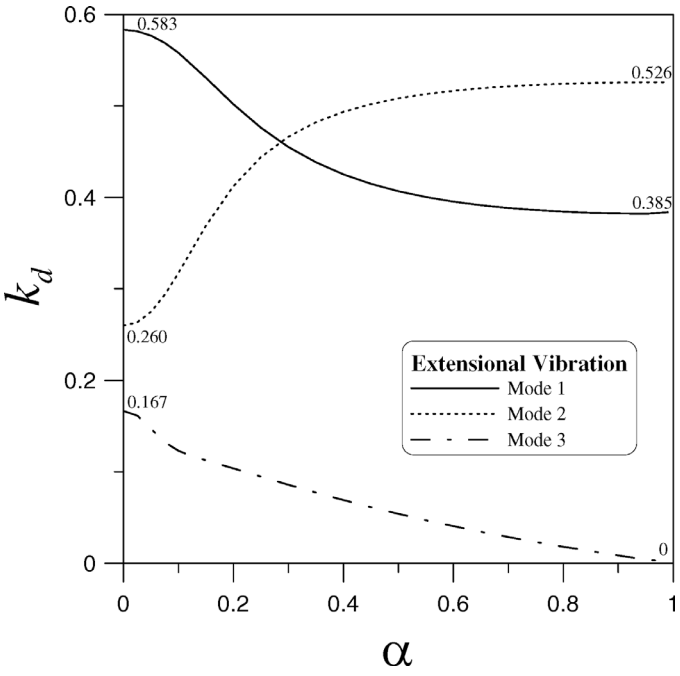

Fig. 11. The value k_d versus α for extensional vibration modes.

true for mode 2, for which R_o and R_i vary in opposite directions. We can see that for $\alpha > 0.287$ the value of k_d for the second mode is greater than that of the first mode.

V. Conclusions

The vibration characteristics of piezoceramic annular disks are important in many engineering applications. However, most of the works for vibration analysis of piezoceramic annular disks published in the literature are analytical and numerical results. Very few experimental results on the full-field configuration of mode shape for piezoceramic disks are available. In this study, the vibration characteristics of piezoceramic annular disks with free-boundary conditions are discussed in detail for transverse, tangential, and radial extensional modes. A self-arranged, amplitude-fluctuation ESPI optical setup with good visibility and noise reduction has been established to simultaneously obtain the resonant frequencies as well as the corresponding mode shapes of transverse and extensional vibrations. The resonant frequencies of piezoceramic annular disks also are measured by the impedance analyzer and LDV for radial extensional and transverse vibrations, respectively. Results have shown that the two optical methods have the advantages of noncontact, real-time, and high-resolution measurement for investigating the vibration problem of piezoceramic annular disks.

From the theoretical and experimental results, we find that only the resonant frequencies of radial extensional vibrations can be measured by impedance analysis. The transverse vibration is investigated using the AF-ESPI and LDV techniques. The vibration modes are classified into two groups (Groups I and II) for transverse and exten-

sional vibrations. The features of Group II are that the resonant frequency will approach infinity as $\alpha \rightarrow 1$. For the extensional vibration, only the first mode belongs to Group I, but Group II includes all the higher order vibration modes. However, the dynamic electromechanical coupling coefficient k_d of all modes for extensional vibrations will approach limit values as $\alpha \rightarrow 1$. It is interesting to note that k_d of the second mode increases when α increases and is greater than that of the first mode for $\alpha > 0.287$.

References

[1] H. F. Tiersten, *Linear Piezoelectric Plate Vibrations*. New York: Plenum, 1969.

[2] *IEEE Standard on Piezoelectricity, ANSI-IEEE Standard 176*, 1987.

[3] A. Iula, N. Lamberti, and M. Pappalardo, "A model for the theoretical characterization of thin piezoceramic rings," *IEEE Trans. Ultrason., Ferroelect., Freq. Contr.*, vol. 43, no. 3, pp. 370–375, 1996.

[4] A. Iula, N. Lamberti, R. Carotenuto, and M. Pappalardo, "Analysis of the radial symmetrical modes of thin piezoceramic rings," *IEEE Trans. Ultrason., Ferroelect., Freq. Contr.*, vol. 46, no. 4, pp. 1047–1049, 1999.

[5] L. Shuyu, "Thickness shearing vibration of the tangentially polarized piezoelectric ceramic thin circular ring," *J. Acoust. Soc. Amer.*, vol. 107, no. 5, pp. 2487–2492, 2000.

[6] T. Takano, H. Hirata, and Y. Tomikawa, "Analysis of nonaxisymmetric vibration mode piezoelectric annular plate and its application to an ultrasonic motor," *IEEE Trans. Ultrason., Ferroelect., Freq. Contr.*, vol. 37, no. 6, pp. 558–565, 1990.

[7] S. K. Ha and Y. H. Kim, "Impedance and admittance matrices of symmetric piezoelectric annular bimorphs and their applications," *J. Acoust. Soc. Amer.*, vol. 108, no. 5, pp. 2125–2133, 2000.

[8] S. K. Ha and Y. H. Kim, "Analysis of an asymmetrical piezoelectric annular bimorph using impedance and admittance matrices," *J. Acoust. Soc. Amer.*, vol. 110, no. 1, pp. 208–215, 2001.

[9] H. A. Kunkel, S. Locke, and B. Pikeroen, "Finite-element analysis of vibrational modes in piezoelectric ceramics disks," *IEEE Trans. Ultrason., Ferroelect., Freq. Contr.*, vol. 37, no. 4, pp. 316–328, 1990.

[10] N. Guo, P. Cawley, and D. Hitchings, "The finite element analysis of the vibration characteristics of piezoelectric discs," *J. Sound Vib.*, vol. 159, no. 1, pp. 115–138, 1992.

[11] N. F. Ivina, "Numerical analysis of the normal modes of circular piezoelectric plates of finite dimensions," *Sov. Phys. Acoust.*, vol. 35, no. 4, pp. 385–388, 1990.

[12] E. A. G. Shaw, "On the resonant vibrations of thick barium titanate disks," *J. Acoust. Soc. Amer.*, vol. 28, no. 1, pp. 38–50, 1956.

[13] U. Minoni and F. Docchio, "An optical self-calibrating technique for the dynamic characterization of PZT's," *IEEE Trans. Instrum. Meas.*, vol. 40, no. 5, pp. 851–854, 1991.

[14] M. Ohki, N. Shima, and T. Shiosaki, "Optical measurement of piezoelectric vibration in circular rod and disk ceramics," *Jpn. J. Appl. Phys.*, vol. 31, no. 9B, pp. 3272–3275, 1992.

[15] B. Koyuncu, "The investigation of high frequency vibration modes of PZT-4 transducers using ESPI techniques with reference beam modulation," *Opt. Lasers Eng.*, vol. 1, pp. 37–49, 1980.

[16] J. R. Oswin, P. L. Salter, F. M. Santoyo, and J. R. Tyrer, "Electronic speckle pattern interferometric measurement of flextensional transducer vibration patterns: In air and water," *J. Sound Vib.*, vol. 172, no. 4, pp. 433–448, 1994.

[17] C. C. Ma and C. H. Huang, "The investigation of three-dimensional vibration for piezoelectric rectangular parallelepipeds by using the AF-ESPI method," *IEEE Trans. Ultrason., Ferroelect., Freq. Contr.*, vol. 48, no. 1, pp. 142–153, 2001.

[18] C. H. Huang and C. C. Ma, "Vibration characteristics for piezoelectric cylinders using amplitude-fluctuation electronic speckle pattern interferometry," *AIAA J.*, vol. 36, no. 12, pp. 2262–2268, 1998.

[19] N. N. Rogacheva, *The Theory of Piezoelectric Shells and Plates*. Boca Raton, FL: CRC Press, 1994.

[20] W. C. Wang, C. H. Hwang, and S. Y. Lin, "Vibration measurement by the time-averaged electronic speckle pattern interferometry methods," *Appl. Opt.*, vol. 35, no. 22, pp. 4502–4509, 1996.

[21] W. P. Mason, *Piezoelectric Crystals and Their Application to Ultrasonics*. New York: Van Nostrand, 1950.

Chi-Hung Huang received his B.S., M.S., and Ph.D. degrees in mechanical engineering from the National Taiwan University, Taipei, Taiwan, in 1987, 1992, and 1998, respectively. Since 1998, he has worked at the Mechanical Engineering Department, Ching Yun University, Chung-Li, Taiwan, Republic of China, as an associate professor.

His research interests include experimental optical measurement and dynamic behavior of piezoelectric materials.

Chien-Ching Ma received the B.S. degree in agriculture engineering, from the National Taiwan University, Taipei, Taiwan, Republic of China, in 1978, and the M.S. and Ph.D. degrees in mechanical engineering from Brown University, Providence, RI, in 1982 and 1984, respectively.

From 1984 to 1985, he worked as a post doc in the Engineering Division, Brown University. In 1985, he joined the faculty of the Department of Mechanical Engineering, National Taiwan University, Taipei, Taiwan, Republic of China, as an associate professor. He was promoted to full professor in 1989.

His research interests are in the fields of wave propagation in solids, fracture mechanics, solids mechanics, piezoelectric material, and vibration analysis

Yu-Chih Lin received the B.S. degree in mechanical engineering from National Taiwan University, Taiwan, Republic of China, in 1994, the M.S. degree in biomedical engineering from National Cheng Kung University, Taiwan, Republic of China, in 1996, and the Ph.D. degree in mechanical engineering from National Taiwan University, Taiwan, Republic of China, in 2004. She currently works in Department of Biomedical Engineering, Yuanpei Institute of Science and Technology, Hsinchu, Taiwan, as an assistant professor.

Her research interests are in the fields of vibration analysis of piezoelectric materials, biomechanics, and human gait analysis.